Pharm Res (2014) 31:3073–3084
DOI 10.1007/s11095-014-1400-9

RESEARCH PAPER

Opening Up the Optical Imaging Window Using Nano-Luciferin

Apurva R. Patel • Ed Lim • Kevin P. Francis • Mandip Singh

Received: 12 February 2014 / Accepted: 28 April 2014 / Published online: 16 May 2014

ABSTRACT

Purpose The objective of this study was to formulate nanoparticles of D-luciferin (Nano-Luc), DiR (Nano-DiR) and dual functional nanoparticles with DiR and luciferin (Nano-LucDiR) for *in-vivo* imaging as well as tracking of the nanoparticles in tumors.

Methods Nano-Luc and Nano-LucDiR were prepared using different lipids, and subsequently characterized for loading and entrapment efficiency, physical properties, release profile, toxicity and stability. We utilized Response Surface Methodology (RSM) to optimize the nanoparticles using design of experiment (DOE Vr.8.0). Nano-Luc was evaluated against free luciferin to establish its pharmacokinetic parameters in mice. *In-vivo* imaging of tumors and tracking of nanoparticles was carried out with an IVIS® Spectrum-CT (Caliper) using xenograft, orthotopic and metastatic tumor models in BALB/c nude mice with different cell lines and different routes of nanoparticle administration (subcutaneous, intraperitoneal and intravenous).

Results Particle size of both Nano-Luc and Nano-LucDiR were found to be <200 nm. Nano-Luc formulation showed a slow and controlled release upto 72 h (90%) *in vitro*. The optimized Nano-Luc had loading efficiency of 5.0 mg/ml with 99% encapsulation efficiency. Nano-Luc and Nano-LucDiR formulations had good shelf stability. Nano-Luc and Nano-LucDiR enhanced plasma half-life of luciferin compared to free luciferin thus providing longer circulation of luciferin in plasma enabling imaging of tumors for more than 24 h. Nano-LucDiR allowed simultaneous bioluminescent and fluorescent imaging to be conducted, with three-dimensional reconstruct of tumors without losing either signal during the acquisition time.

Conclusion Nano-Luc and Nano-LucDiR allowed prolonged reproducible *in-vivo* imaging of tumors, especially during multimodality 3D imaging.

KEY WORDS enhanced *In-vivo* imaging · luciferin · nanoparticles · theranostic · tumor imaging

ABBREVIATIONS

CCD	Central Composite Design
CT	Computed Tomography
DOE	Design Of Experiment
DSC	Differential Scanning Calorimetry
FOV	Field Of View
IP	Intraperitoneal
IV	Intravenous
Nano-DiR	Nanoparticles of DiR
Nano-Luc	Nanoparticles of D-Luciferin
Nano-LucDiR	Nanoparticles with DiR and Luciferin
NCs	Nano lipid carriers
QbB	Quality by Design
ROI	Region of Interest
RSM	Response Surface Methodology
SD	Standard Deviations
SQ/SC	Subcutaneous
TPGS	α-Tocopherol Polyethylene Glycol Succinate
Xenolight DiR	DiIC18(7) or 1,1′-dioctadecyltetramethyl indotricarbocyanine iodide

INTRODUCTION

Imaging techniques are routinely used in medical practice and clinical trials (1–4) for non-invasive diagnosis of disease progression and treatment. With recent advancements in imaging technologies, preclinical molecular imaging is becoming an integral part of research and development in medical science (5,6). Non-invasive *in-vivo* imaging techniques have been essential to study changes within organs, tissues, cells, or at molecular level in animal models due to physiological or environmental factors. In particular, tumor imaging provides several advantages, such as 1) better prediction of disease progression (7), 2) untangle the biological

Electronic supplementary material The online version of this article (doi:10.1007/s11095-014-1400-9) contains supplementary material, which is available to authorized users.

A. R. Patel • M. Singh (✉)
College of Pharmacy and Pharmaceutical Sciences
Florida A&M University, Tallahassee, Florida 32307, USA
e-mail: mandip.sachdeva@famu.edu

E. Lim • K. P. Francis
Caliper - A PerkinElmer Company, Alameda, California 94501, USA

complexities of tumors (feasibility of longitudinal measurements, three-dimensional maps of tumor, *etc.*) (8), 3) visualization of different biological aspects of metastasis (9,10), 4) strategies to alter the tumor microenvironment and interpret them into improved cancer detection (11,12), 5) tailored cancer therapeutics to match individual needs (5), 6) streamline cancer drug development (5,13), 7) identifying potential drug targets on tumors and translate into new therapies in humans (13).

Preclinical imaging techniques can be classified into morphological/anatomical [high-frequency micro-ultrasound, magnetic resonance imaging (MRI) and computed tomography (CT)] and more functional molecular imaging techniques [optical imaging (fluorescence and bioluminescence), positron emission tomography (PET), and single photon emission computed tomography (SPECT)] (14). Each technique has its own advantages and limitations. To overcome these limitations and gain further advantage, multimodal systems have been developed by utilizing the advantages of anatomical modalities (CT/MRI) with the functional imaging (optical imaging/PET/SPECT) (7,9,15).

Bioluminescence imaging is a noninvasive and cost-effective method which allows real-time observation of complex biological activity in live animals (16–18). Bioluminescence imaging is based on the introduction and expression of a gene construct to produce a protein "luciferase", which is an enzyme that converts D-luciferin to oxyluciferin and light emission which provides the imaging contrast (19–21). Bioluminescence imaging in animal models is routinely conducted using firefly luciferase. Other luciferases used besides the firefly variety are Renilla luciferase (22) and bacterial luciferase (23,24). Due to their unique substrate specificity and characteristics (25), they can be used simultaneously. The substrate "luciferin" is usually given as an intravenous (IV) or intraperitoneal (IP) injection to animals for imaging purposes. Less common methods for luciferin delivery include using an osmotic pump (26) or introducing the substrate into the animals drinking water (27). Due to faster clearance of luciferin from plasma, there is a relatively short imaging window where stable light emission can be recorded (28), while multiple injections complicate the imaging parameters by altering variables such as luciferin PK/PD. In an effort to overcome these problems, researchers have reported continuous delivery of luciferin to enhance temporal resolution by use of osmotic pumps (26,29) or liposomal delivery to increase radiance (30).

We encapsulated luciferin within a lipid nanocarrier system (Nano-Luc) for prolonged delivery of this substrate within the animal once administered *via* IV, IP or subcutaneous (SQ) route. Lipid nanoparticles have been shown to protect the active ingredients from enzymatic degradation, provide controlled release of drug, and enhance the therapeutic effect and stabilization of chemically unstable drugs due to their lipid matrix (31–33). Along with the Nano-Luc, we also developed nanoparticles containing luciferin in combination with the near infrared dye DiR (Nano-LucDiR), the latter combination allowing imaging of tumors and their neovascularization.

The efficiency and stability of Nano-Luc and Nano-LucDiR were evaluated in nu/nu and Balb/c mouse models injected with tumor cells (lung and breast tumor cells) expressing a luciferase reporter gene (12,21,34). We analyzed the formulation for drug loading, entrapment efficiency and release of luciferin. Factors that influence these parameters, such as lipid components, ratio of lipids/oil/surfactant and process variables were evaluated and optimized through quality by design approach (QbD). We also evaluated the formulations for stability by accelerated stability studies and differential scanning calorimetry.

MATERIALS AND METHODS

Materials

Luciferin and Xenolight DiR (DiIC18 (7) or 1, 1′-dioctadecyltetramethyl indotricarbocyanine Iodide) were provided by Caliper - a PerkinElmer Company (Alameda, CA). Lipids (such as monosteol, precirol, gleol, MCT oil, transcutol and miglyol) were kind gift samples from Gattefosse (Saint Priest, France). Dialysis bags with molecular weight cut off range of 6,000–8,000 daltons with flat width of 23 mm was obtained from Fisher Scientific (Pittsburg, PA). Vivaspin centrifuge filters with molecular weight cut off range of 10, 000 daltons were obtained from Sartorius Ltd, (Stonehouse, UK). Fetal bovine serum (FBS), antibiotics were purchased from Invitrogen Corp (Eugene, OR). Lung cancer cell lines (A549-luc, H460-luc) and breast cancer cell lines (4 T1-luc, MDA-MB-231-luc) were obtained from Caliper (Alameda, CA). The cells were maintained with supplemented media at 37°C in the presence of 5% CO2 in air. All other chemicals used in this research were of analytical grade.

Animals

Female nu/nu and Balb/c mice (20–25 g; Charles River Laboratories Wilmington, MA, USA) were utilized for the studies. The protocol for *in-vivo* experiments was approved by the Institutional Animal Care and Use Committee, Caliper, Alameda CA. The animals were acclimated to laboratory conditions for one week prior to experiments and were given an alfalfa-free animal chow and water *ad libitum*. The temperature of the room

was maintained at 22±1°C and the relative humidity was found in the range of 35–50%.

Preparation of Nano-Luc and NanoLuc-DiR

Nano-Luc and Nano-LucDiR were prepared by hot melt homogenization (35). In brief, luciferin and/or Xenolight DiR were dissolved in methanol and mixed with different lipids. Later, the organic solvent was removed by rotary evaporator for 30 min at 60°C. The lipid phase was mixed with the aqueous phase at pH 7.0 (20 ml) containing surfactant (such as tween 80 and tween 20) (Table S1) using a Cyclone IQ2 with Sentry™ Microprocessor (USA) at 20,000 rpm for 15 min. This mixture was passed through Nano-DeBee® (BEE International, South Easton, MA) at 20,000–30,000 psi for three to five cycles. Throughout the process, temperature was maintained at 60°C.

Response Surface Methodology (RSM)

A response surface design was used to evaluate response behavior at variables studied in the experimental region using polynomial equation. The conditions that determine the improvement of process and product development were studied using RSM (36). The objective of this study was to select the lipid, oil and surfactant for the Nano-Luc formulation with the desired response. The particle size, entrapment efficiency, loading efficiency and release rate at 24 h were dependent variables and actual values of independent variables are shown in Table S1. The parameter level selection was based on a preliminary study and on findings in the literature (Table S1). Design- Expert software (DOE V. 8.0, Stat-Ease Inc., Minneapolis, MN, USA) was utilized for the statistical experimental design.

Central Composite Design

A further optimization of selected variables based on the RSM response was done by using central composite design to optimize compositions of variable factors and to evaluate interaction and quadratic effects of the factors on characteristics of Nano-Luc. Lipid and oil concentrations were selected as significant factors based on the RSM optimization desirability study results. Each of the factors was tested at 5 different levels and 5 center points were included. DOE V.8.0 was used for the design, analysis and plotting of the various 3D and contour graphs.

Optimization of Responses Using Desirability Function

The entrapment efficiency and loading efficiency were targeted to maximum, while particle size and release rate were limited to <200 nm and <50% respectively, in the procedure, as these values confirm the desired product outcome. The desirability for each response (di) was calculated at a given point in the experimental domain based on desirable ranges for each response. The desirability function (an objective function in multiple response method) of these parameters was calculated using DOE V.8.0, where optimum is the point with the highest value for the desirability.

Characterization of Nano-Luc and Nano-LucDiR

Nicomp 380 ZLS (Particle Sizing Systems, Port Richey, FL) was used to measure particle size and zeta potential of nanoparticles. To measure the entrapment efficiency, Nano-Luc (0.5 ml) was placed on top of the vivaspin centrifuge filter membrane (molecular weight cut-off 10,000 Daltons) and centrifuged for 20 min at 5,000 rpm. About 20 µl flow-through was collected out of 500 µl at the bottom of vivaspin filter and absorption was measured at 327 nm to determine the luciferin content. The drug loading was determined by centrifuging 1.0 ml of formulation at 16,000 g for 1.5 h and sediment was dissolved in tetrahydrofuran. The content of luciferin was measured by absorption at 327 nm. Drug loading was calculated using following equation (37)

$$\text{Luciferin Content}\left(\%\frac{\text{w}}{\text{w}}\right) = \frac{\text{mass of Luciferin in nanoparticle} \times 100}{(\text{mass of nanoparticle recovered})} \quad (1)$$

Drug Release Studies

Drug release studies were performed using USP 1 (basket) dissolution apparatus (Vankel, NC). Briefly, 1 ml of nanoparticle formulation was placed in a soaked cellulose membrane (6,000–8,000 molecular weight cut off) and ends were closed and placed inside the basket. The dissolution media (200 ml) was phosphate buffer saline (PBS) pH 7.4 containing 0.5% *w/v* Volpo-20 and 0.5%*v/v* Tween 80. The baskets were rotated at 50 rpm for 72 h at 37.0±0.1°C. The samples (0.5 ml) were collected at different time points with replacement of equal dissolution media and luciferin content was measured at 327 nm.

Differential Scanning Calorimetry

The interaction of luciferin and Xenolight DiR with lipids and their association within Nano-Luc and Nano-LucDiR were evaluated using a DSCQ100 (TA instrument, DE). The thermal pattern was determined against empty pan from 0°C to 300°C at 5°C.min^{-1} heating rate for different samples weighed and sealed in an aluminum hermetic pan. Transition temperatures and transition enthalpies were

determined from the endothermic peak minima and by integration of the endothermic transitions using linear baselines, respectively.

Accelerated Stability Studies

Nano-Luc and Nano-LucDiR were stored at different temperatures 30±1°C, 40±1°C and 50±1°C; and also at room temperature (mean temperature being 25.7±0.6°C) for a month (38). Aliquots were removed after intervals of time (0, 7, 14, 21 and 30 days) and formulations were analyzed for particle size, entrapment efficiency, release rate and luciferin content by methods mentioned above. The slope of the log percent luciferin remaining *vs* time plot curve was used to determine degradation rate constant (K) using following the equation:

$$Slope = \frac{K}{2.303} \tag{2}$$

Where, K is the degradation rate constant.

In-vitro Comparison of Nano-Luc and Luciferin

Nano-Luc was compared with free luciferin against luciferase expressing cells for bioluminescence. Also, Nano-Luc was tested for cytotoxicity against primary cells and cancer cells. Luciferase activity was determined by luciferase reporter assay system. Cells were plated into 96 well plates with 10^4 cell per well and treated with Blank Nano-Luc (without luciferin) and Nano-Luc. Viability of cells was determined after 24 h using crystal violate assay. The percentage viability was compared to the control (no treatment). For bioluminescence system, Nano-Luc and luciferin were incubated with different number of cells for 30 min and bioluminescent was measured for luciferase activity using luminometer (Tecan M200, Tecan Inc., USA). Each experiment was repeated three times.

In-vivo Tumor Models

In-vivo tumors for the current study were grown using lung cancer cells (A549 & H460) and breast cancer cells (4 T1 & MDA-MB-231). All the cell lines were modified for the luciferase reporter gene expression as reported earlier by Lim et. al (21).

Xenograft Tumor Model

The adherent tumor cells, A549-luc and H460-luc2 were washed with PBS, harvested from confluent cultures using 0.25% trypsin and 0.02% EDTA solution. Trypsin was neutralized with medium containing 10% FBS. The cells were centrifuged and resuspended in medium containing 10% FBS. The numbers of viable cells were determined by trypan blue assay and concentrations of 2×10^6 cells/50 µl were prepared in growth medium. The cell suspension (50 µl) was injected subcutaneously into flank areas of each mouse. Mice were randomized into control and treatment groups (each group having six animals and experiments were in replicates) when xenografts were palpable with a tumor size of 50 mm^3.

Orthotopic Tumor Model

The orthotopic tumor model was used to mimic the cancer in humans in athymic nu/nu or Balb/c mice (6–8 week old). Animals were anesthetized with 2% isoflurane and placed in the supine position. 4 T1-luc2 cells were implanted into the mammary fat pad by injecting 1×10^6 cells in a volume of 20 µl. Mice developed tumors in 7–10 days after inoculation of the cells and were randomized in various groups 10 days post tumor implantation. Mice were randomized into control and treatment groups (each group had six animals and experiments were in replicates).

Metastatic Tumor Model

Tumor metastasis was established using an intracardiac injection of MDA-MB-231-luc cells. Mice were anesthetized with 2% isoflurane and placed in the supine position. A 29-gauge needle attached to a 0.3 mL syringe was inserted into the second intercostal space 3 mm to the right of the sternum and aimed centrally. The syringe plunger was pulled back slightly while slowly advancing the needle. A continuous entrance of red oxygenated blood into the transparent needle hub indicated proper positioning of the needle into the left ventricle. 1×10^6 MDA-MB-231-luc cells in 20 µL were slowly injected over a 20–40 s period. Mice were randomized into control and treatment groups (each group had six animals and experiments were in replicates).

In-vivo Imaging

Bioluminescence/Fluorescence Imaging

Mice were anesthetized with 2% isoflurane and imaged for different time points up to 24 h following IP, IV and SQ injection of 15 mg/kg luciferin, Nano-Luc (equivalent to 15 mg/kg of luciferin) and Nano-LucDiR (equivalent to 15 mg/kg of luciferin). Imaging was performed with an IVIS Spectrum (21). For kinetic studies, mice were continuously imaged at 5 min intervals for upto 2 h to determine peak luciferase signals. Bioluminescent signals were quantified using Living Image® software (Caliper, Alameda, CA.).

Tumor Multimodality (CT/DLIT/FLIT) Imaging

Mice were anesthetized with 2% isoflurane and imaged following IP, IV and SQ injection of Nano-LucDiR (equivalent to 15 mg/kg of luciferin). Imaging was performed with an IVIS Spectrum-CT (10). For kinetic studies, mice were continuously imaged at 5 min intervals for up to 2 h to determine peak luciferase (open filter) and fluorescent (exCitation 745 nm, emission 800 nm) signals. Bioluminescent and fluorescent signals were quantified using Living Image® software (Caliper, Alameda, CA.).

Statistical Analysis

Data were represented as mean ± standard deviations (SD) and model parameters as estimates±standard errors (SE). Means were compared between two groups by student's *t* test and between three dose groups by one-way variance analysis (ANOVA). Probability (p) values<0.05 were considered significant. All statistical analyses were performed using GraphPad Prism® 5.0 software (San Diego, CA).

RESULTS

Experimental Design and Effect of Variables on Response

In this study, luciferin containing nanoparticles were prepared using a hot melt homogenization method. The experimental runs with variables and corresponding responses for the 32 formulations were tested (Table S2). The mean particle size ranged from 149 nm to 210 nm depending on the factor level selected during preparation. The response surface quadratic model was used for analysis purpose. Statistical analysis revealed that none of the factors were significant to influence mean particle size (Y1), as shown in Table S3. The mean particle size measured and reported was at 95% confidence interval representing 95% particles in the colloidal systems. Also, zeta potential for different formulations ranged from 28 ±4 mV to 42±3 mV. The entrapment efficiency was represented in percentage of loading efficiency and it ranged from 82% to 99% depending on the factor level selected during preparation. The response surface quadratic model with inverse transform was used for analysis purpose. Statistical analysis revealed that oils were the significant factor to influence entrapment efficiency (Y2) (Table S3). The loading efficiency (Y3) of Nano-Luc was in range of 56to 92%. The most significant factor affecting the loading efficiency was shown to be oils ($p<0.05$) followed by lipids ($p<0.05$) used in the preparation of Nano-Luc. An increase in release rate was observed with increase in luciferin concentration. Lipids were also shown to significantly influencing the release rate. Affect of Lipid and Oil type factors on loading efficiency, entrapment efficiency, 24 h release rate and mean particle size are shown in Figure S1.

Central Composite Design

After the lipids and oils were found as critical factors based on the screening design, a 2-factor with 5-level central composite design was applied to optimize these factors (Table S4). This method comprised of 2 groups of design points, including 2-level factorial design points, axial points and center points (39). To determine the main, interaction and quadratic effects of the solute and soluplus concentrations on the selected responses, 2 independent factors were studied over 5 different levels, coded as -α, −1, 0, 1, and+α. The value for alpha (1.414) was intended to fulfill the rotatability in the design. The other variables were fixed at the following values: luciferin (100 mg); surfactant (480 µl). The experimental runs with formulation variables and corresponding responses for the 13 tested formulations are presented in Table S4. The best fit for each of the responses was found for the quadratic models of Y1 and Y2, and the linear model of Y3. The statistical analyses for response following models analysis were describe as the effect of various factors on the tested responses (Table I). Contour plots and three-dimensional response surfaces were drawn to estimate the effects of the independent variables on each response (Figure S2). The overall desirability response was evaluated based on individual desirability of each responses using DOE v8.0.7. The optimized composition with a desirability value of 0.968 was identified (Fig. 1).

Differential Scanning Calorimetry

For the free luciferin, the thermogram revealed a small, clear event at about 197°C (Figure S3-A), which emphasizes the crystalline melting point of luciferin. No melting was observed before or during the process which can therefore most likely be attributed to a solid–solid phase transformation. The new modification was stable upon cooling. Upon further heating, a very pronounced DSC endothermic peak appeared at about 237°C (Figure S3-A), and subsequently, the drug decomposed and turned black. The DSC thermogram of precirol (Figure S3-D) and monosteol (Figure S3-B) showed a sharp endothermic peak at about 63°C, with addition of miglyol (Figure S3-F) and luciferin there was a depression in the endothermic peak because they behave as impurities. Also, DSC studies confirmed the absence of drug excipients interactions, as shown by thermograms of Nano-Luc (Figure S3-C) and Nano-LucDiR (Figure S3-E). Dissappearance of endothermic peak of luciferin in nanoparticles shows that luciferin is in amorphous form and points an interaction between lipids and luciferin.

Table I Statistical Analysis of Entrapment Efficiency (X1), Loading Efficiency (X2) and 24 h Release rate (X3) in the Central Composite Design

	X1: Entrapment Efficiency		X2: Loading Efficiency		X3: 24 h Release Rate	
	EC	*p* value	EC	*p* value	EC	*p* value
Intercept	85.454	N/A	74.2	N/A	0.01780	N/A
A-Monosteol	14.0790	0.0046	2.6497	0.4148	0.0049	0.0002
B-Miglyol	−1.4172	0.6930	21.6981	0.0002	−0.0028	0.0053
AB	0.6525	0.8972	0.89	0.8428	−0.0016	0.1389
A^2	−1.9776	0.6089	5.9443	0.1127	0.0014	0.1094
B^2	0.1773	0.9630	−6.3331	0.0947	0.0016	0.0632

EC (Estimated Coefficient); * Significant values at $p < 0.05$

Stability Studies

Accelerated stability studies based on the parameters, such as particle size, loading efficiency and entrapment efficiency were conducted on Nano-Luc. The particle size during the one month storage was slightly increased from the 172±8.62 nm to 188.56±7 .80 nm with PDI changed to 0.348±0.01 from 0.330±0.06. The entrapment efficiency and loading efficiency of Nano-Luc initially was found to be 97.79±2.68% and 96.12 ±3.86% and after a month was found to be 96.59±0.54% and 94.12±2.34% indicating that the drug wasn't leached out from nanoparticles for the period of time. Also, the accelerated stability studies at 30°C, 40°C and 50°C were conducted and percent recovery of luciferin from Nano-Luc was measured at different time points (Figure S4). The degradation rate constant (k) for the percent recovery of luciferin from Nano-Luc were 0.000691, 0.016121 and 0.116762 at 30°C, 40°C and 50°C, respectively. On storage of the Nano-Luc, there were no significant changes in the particle size, PDI and entrapment efficiency of the nanoparticles at 30°C. There was decrease in entrapment and loading efficiency at 50°C, since the melting point as confirmed by DSC (Figure S3) was near 60°C and possible reason for this could be alteration of lipid matrix and leaching of luciferin from caged matrix.

In-vitro Analysis of Nano-Luc

The cytotoxicity of Nano-Luc was determined against primary cells (*e.g.* primary lung epithelial cells, smooth muscle cells) and cancer cells by incubating with various concentrations of formulation for 24 h. *In-vitro* cytotoxicity results showed a non-toxic nature of Nano-Luc at concentration range of 10–500 µg/ml. There was no statistical difference in percentage cell kill between treated groups compared to control (no treatment) and cell viability was more than 95% in all groups. For bioluminescence assay comparison of Nano-Luc and luciferin, free luciferin showed higher luminescence flux than Nano-Luc depending on the cell numbers the fold increase varied over the range of 2–11 fold (Figure S4), indicating that luciferin is tightly caged inside the nanoparticles.

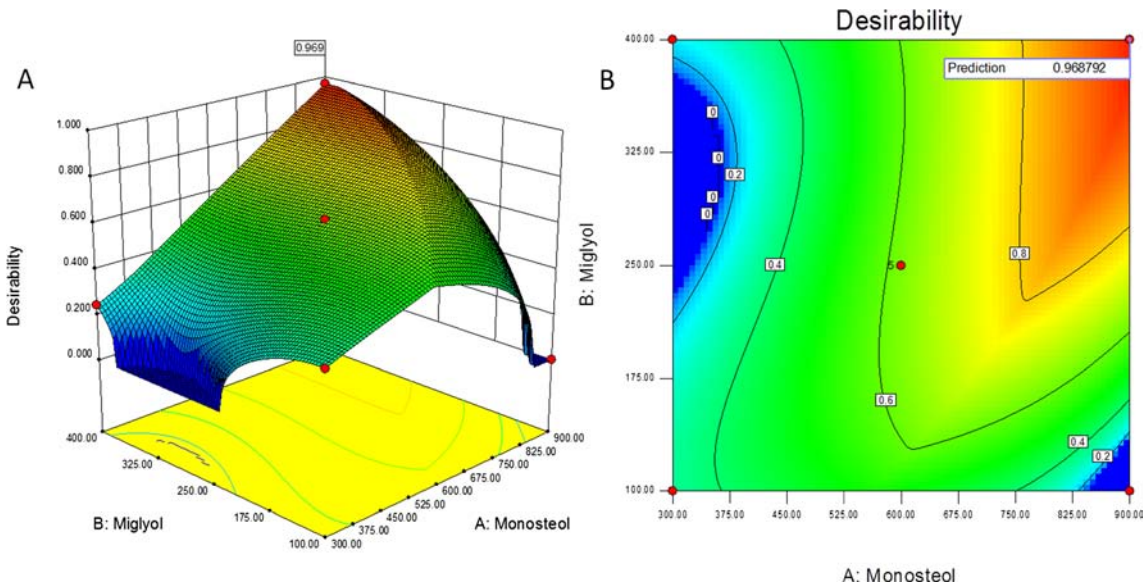

Fig. I Response surface plot (**a**) and countor plot (**b**) of desirability function.

In-vivo Imaging and Kinetics of Free Luciferin and Nano-Luc/Nano-LucDiR

For all tumor models, circulation of free luciferin was shorter compare to Nano-Luc, IV administration of Nano-Luc showed faster release compared to Nano-Luc administered by IP/SC over time observed. Bioluminescence intensities were estimated based on the region of interest (ROI) on each tumor. The bioluminescence images were then quantified and used to evaluate the pharmacokinetics of free and Nano-Luc luciferin in 4 T1-luc tumor models (Figure S5). The images for Nano-Luc were compared to that of free luciferin for the corresponding animal models based on a normalized intensity color map and total injected luciferin, (Figure 2 & 3).

Bioluminescent signals taken every 5 min over a period of 120 min in a 4 T1-luc model showed that free luciferin was cleared from circulation within 60 min (Fig. 3). Free luciferin was found to have a rapid clearance and similar kinetic was observed in all models (Fig. 3), while IP/SC delivery of Nano-Luc showed an estimated $t_{1/2}$ value of more than 3 h. Intravenous Nano-Luc, showed a two phase release kinetic, a rapid release in the early phase ($t < 30$ min) followed by a slower steady release kinetic (Fig. 3). Bioluminescence resulting from the injection of Nano-Luc increased over the one h and remained steady for another 4 h. The signal then slowly declined over the next 20 h to a low, yet detectable level at 24 h. In comparison, with free luciferin, a rapid increase in bioluminescence was seen during the first 30 min, followed by a rapid decline over the subsequent 30 min. Luciferin loaded in Nano-Luc had a 400-fold greater phase II half-life in circulation as compared to free luciferin.

In-vivo Imaging and Kinetics of Nano-LucDiR

Figure 4 shows a CT image with overlaying 3D bioluminescent and fluorescent tumor signals of a 4 T1-luc tumor model following administration of Nano-lucDiR. A 3D construct for the tumor was build and it shows the differential imaging signals as shown in video (Video 1). With respect to the kinetics of luciferin, we observed similar trend as compared to Nano-Luc for release of luciferin and expression of bioluminescence intensities from Nano-LucDiR formulations (Fig. 5). Also, florescence intensities for DiR were steady over the period of time (Fig. 5).

DISCUSSION

In the present study, we have developed novel nanocarriers for bioluminescent pre-clinical imaging of cancer using luciferin. This is the first study to report use of nano lipid carriers for the delivery of luciferin and enhanced *in-vivo* imaging. Bioluminescence is a well-known system for non-invasive *in-vivo* analysis of molecular and cellular events being easy, cost-effective, sensitive and robust (8,11). Luciferin (a firefly luciferase substrate) has permeability co-efficient of 3.6×10^{-9} cm.s^{-1} and a very short half-life of 5.33 min (30). Also, with faster clearance of luciferin from plasma and limitation of multiple injection of luciferin (30), it limits the luciferin based imaging applications. Thus, we proposed controlled sustained release of luciferin with effective radiance for imaging over the period of 24 h. The triglycerides such as monosterol, precirol and Miglyol were used to prepare the Nano-Luc system. We utilized a QbD approach in designing stable formulation for enhanced *in-vivo* imaging.

Monosteol and precirol were chosen as suitable lipids for Nano-Luc due to the higher solubility and partitioning. We have used triglycerides prepare the nanoparticle formulation, where Monosteol and precirol form the solid outer shell of the nanoparticles. Miglyol (caprylic/capric triglycerides) is a liquid lipid, known to enhance the encapsulation of lipophilic drugs in the nanoparticles. Furthermore, addition of Miglyol tends to promote the formation of a small particle. Based on the chemical nature of the lipid molecules, the inner structure of nanoparticle is different from that of solid lipid nanoparticles and made of mixtures of solid and liquid lipids. The solubility of lipophilic ingredients in oils is generally much higher than in solid lipids. Mono, di, and triglycerides rich lipids can help the solubilization of luciferin in the lipid fraction, and miglyol provides extra space for luciferin to get

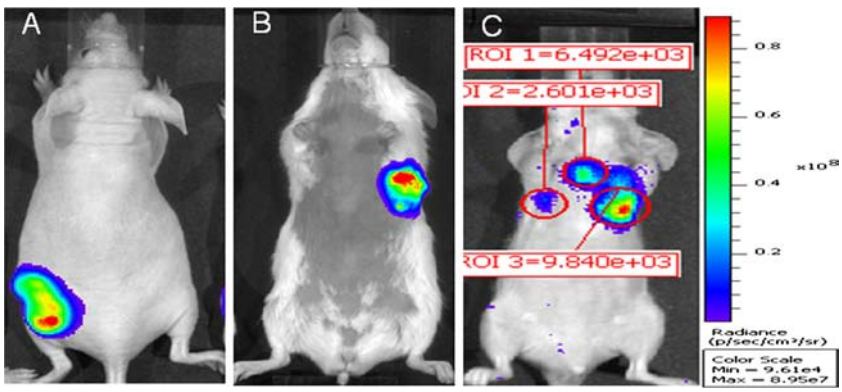

Fig. 2 Nano-luc tumor imaging in mice with (**a**) subcutaneous H460-luc2 tumors, (**b**) orthotopic 4 T1-luc2 tumors and C) mb231-luc2 metastatic tumors using 15 mg/kg luciferin equivalent Nano-Luc by IV at 2 h.

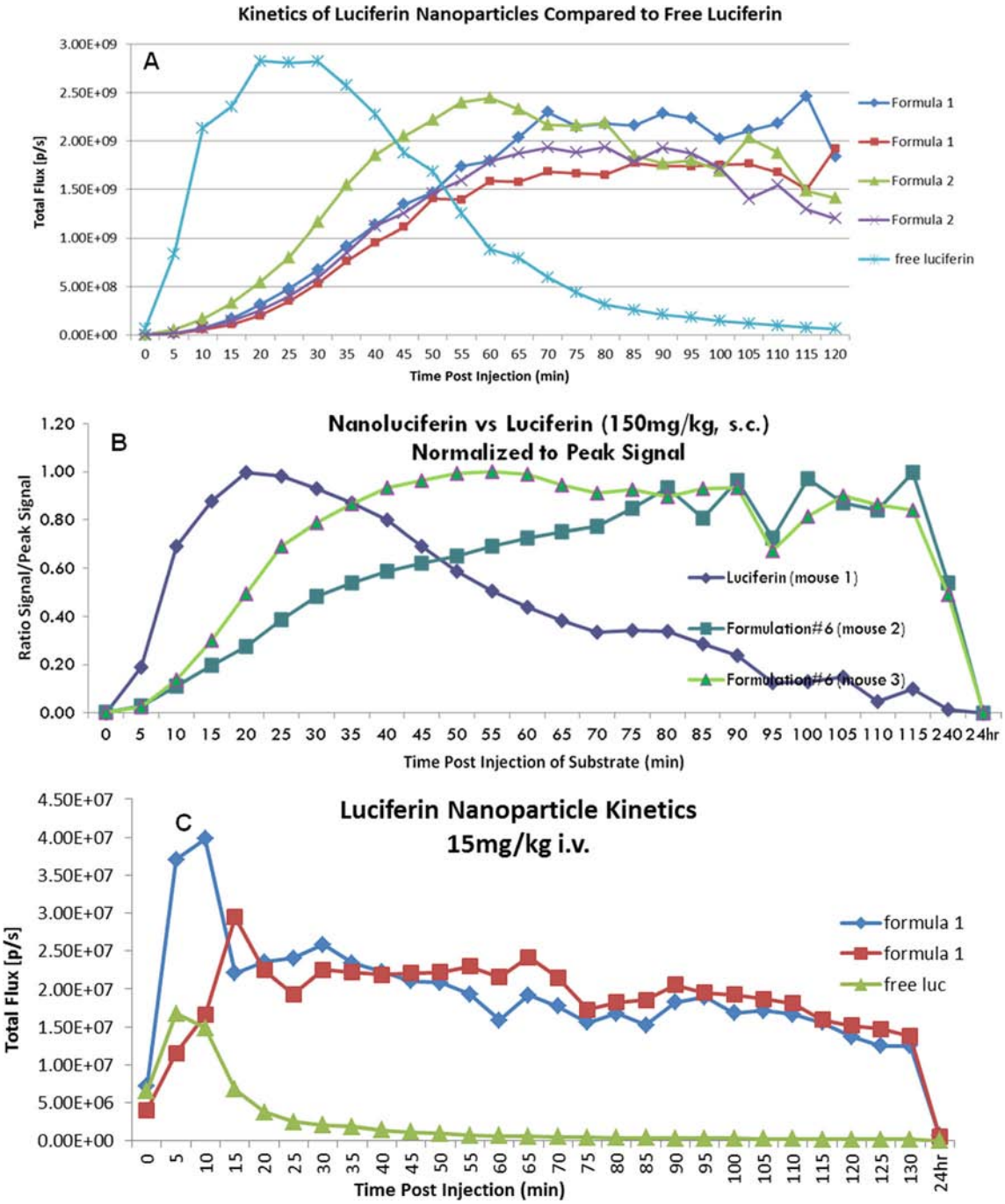

Fig. 3 *In-vivo* kinetics of Nano-luc compared to free luciferin. (**a**) Total flux of bioluminescence *Vs* time plot following IP injection of Nano-Luc and free luciferin. (**b**) Normalized to peak signal flux *Vs* time plot following subcutaneous injection of Nano-Luc and free luciferin. (**c**) Total flux of bioluminescence *Vs* time plot following IV injection of Nano-Luc and free luciferin.

entrapped, thus increasing luciferin loading capacity and minimal expulsion during storage could be achieved by the development of Nano-Luc (40). The liquid state of Miglyol oil helps to encapsulate the higher amount of Luc and reduces the particle crystallinity which imparts better stability and higher suitability for controlled release. For the optimization of Nano-Luc, RSM experimental design showed a significant correlation between dependent and independent factors. Quadratic model was found to be the most suitable for defining the relationship for some of the responses (model F value <0.05; lack of fit value >0.05 as per one-way ANOVA) (Table S3). Central composite design showed a strong relationship between lipid concentrations and response variable entrapment efficiency, loading efficiency and release of luciferin from Nano-Luc. After the analysis of data, optimization using DOE Vr 8.0.7 software was done to get a particle size of

Fig. 4 Spectrum CT/DLIT/FLIT imaging of subcutaneous tumor model in mice followed by NanoLuc-DiR (dual chromospheres- DiR & luciferin) for detection of tumor multimodality at 2 h .

less than 200 nm with maximum entrapment efficiency and loading efficiency with 50% drug release at 24 h. The intention behind these selections was to provide controlled sustained release of luciferin. Using these criteria, the 3 variables were then combined to determine an overall optimum design. Figure S1 shows an acceptable region that describes the requirements of these responses. This optimum region could therefore be used to construct the design space of Nano-Luc with high quality characteristics. A further central composite design optimization and validation process was then undertaken using desirable characteristics (Fig. 1) that depended on the prescriptive criteria of maximum entrapment efficiency, maximum loading efficiency and release rate.

The DSC thermograms of Monosteol, Miglyol, Precirol and Nano-Luc are represented in Figure S3. The DSC study showed no chemical interaction between luciferin and excipient. Luciferin endothermic peak was not seen in DSC thermogram of Nano-Luc with most likely reason being the molecular inclusion of luciferin in the lipid matrix. Similar results have been reported earlier by other researchers (41,42). The DSC thermograms of Nano-Luc showed broadening of lipid peak, which may be due to the excipients being heated and cooled for several cycles, larger surface area due to the smaller size of the particles and also Miglyol, Luciferin and surfactant which behave as impurities. Similarly, Puglia *et al.* (43) reported that the incorporation of ketoprofen/naproxen into the lipid formulations resulted in the broadening of the lipid endothermic peak. The stability data indicated that the lipids contributed to the stabilization of the formulation and could be useful for improving the shelf life of Nano-Luc. This might be attributed to the fact that transformation of colloidal suspension into solid form has the advantage of preventing particle aggregation, degradation reactions (hydrolysis), and preventing the leakage of the luciferin. Furthermore, the shelf-life of Nano-Luc estimated at 25°C was more than 10 months, while at 8°C it was more than 2 years. Furthermore, *in-vitro* cytotoxicity assay showed that Nano-Luc was non-toxic and safe to use. Also, *in-vitro* bioluminescence assay confirmed that luciferin was caged inside the matrix of nanoparticles.

To evaluate the *in-vivo* effectiveness of Nano-Luc, nanoparticles were administrated *via* SC, IP and IV route into mice having tumors expressing luciferase. Luciferin encapsulated in Nano-Luc remained in the circulation giving bioluminescent radiance suitable for imaging for more than 24 h. SC & IP administration of Nano-Luc demonstrated slow release of luciferin *in-vivo* compared to free luciferin with peak intensity lower than that of free luciferin. This phenomenon was also observed by Gross *et al.* (26) for osmotic pump delivery of luciferin. With IV administration, flux efficiency of Nano-Luc luciferin was higher than that of free luciferin, which may be due to faster clearance of free luciferin than Nano-Luc. A slow release in the second phase compared to initial rapid release of luciferin from Nano-Luc was most likely due to the release of the entraped luciferin. The total luciferin that was initially associated with the outer core of nanoparticles (40) was probably the reason for the early rapid release observed for luciferin in Nano-Luc. The osmotic pump delivery approach by Gross *et al.* (26) requires surgical implantation of device, whereas with our approach all that is necessary is a simple injection by SC/IP/IV route. As per Azadeh *et al.* (30), intravenously injected long circulating luciferin liposomes provided sufficient radiance for more than 12 h of imaging, while Nano-

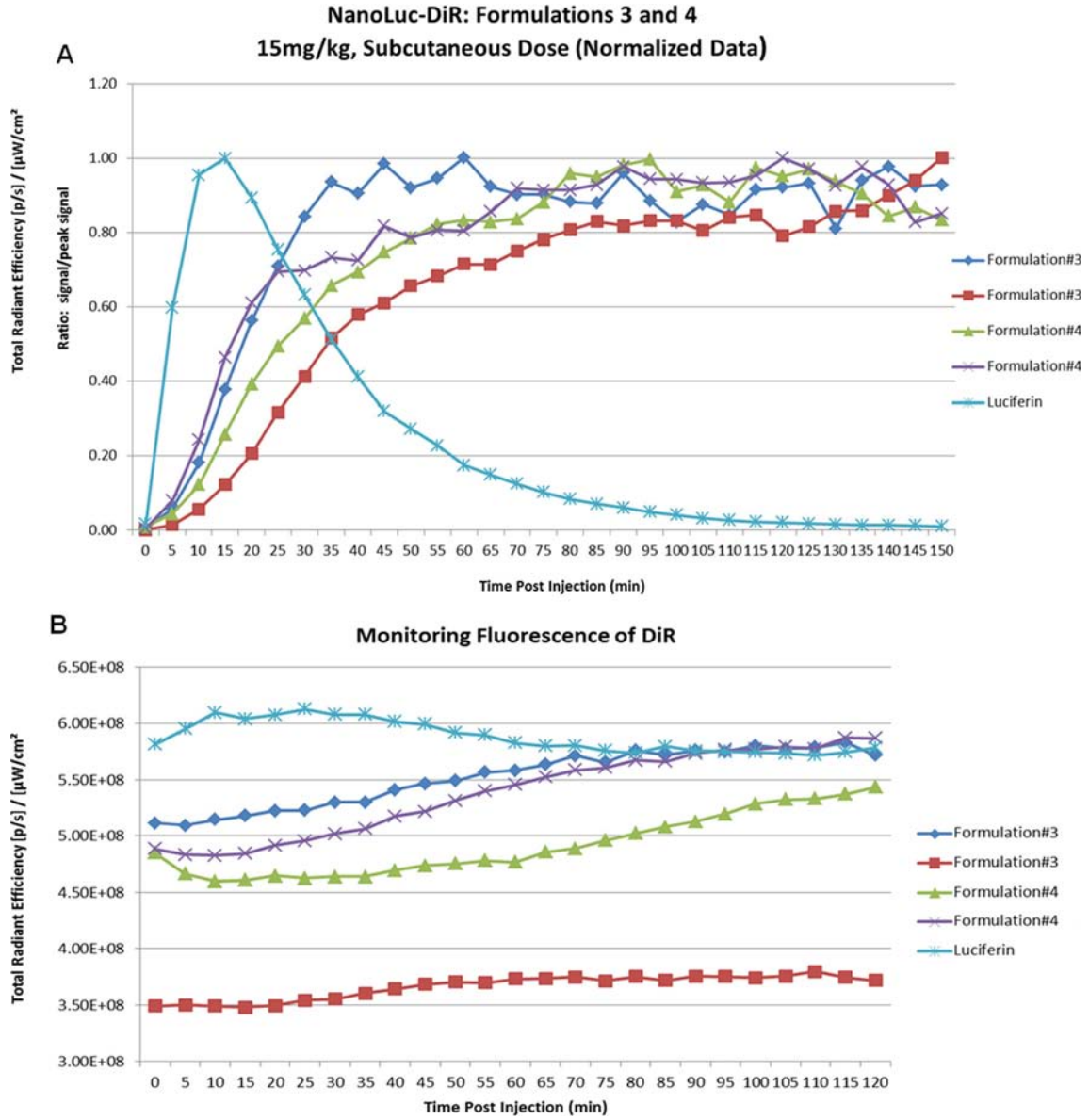

Fig. 5 *In-vivo* kinetics of Nanoluc-DiR compared to free luciferin. (**a**) Normalized to peak signal flux *Vs* time plot following subcutaneous injection of Nanoluc-DiR and free luciferin. (**b**) Total flux of fluorescence *Vs* time plot following dose of Nanoluc-DiR.

Luc provided sufficient radiance for 24 h. Also, bioluminescence kinetics was steady over the period of 4 h with our formulation at peak flux. Recent research conducted with osmotic pump delivery showed release and imaging possible for 48 h but raw bioluminescence compare to free luciferin was 70–150 folds lower (26) and photon count for bioluminescence signal with osmotic pump was not steady. Azadeh *et al.* (30) used ultrasound to induce local hyperthermia, to heat the tumor area at 42°C, to increase the raw bioluminescence radiance leading to ~75 times (without hyperthermia) and ~25 times (with hyperthermia) less bioluminescence radiance compare to free luciferin. Our formulation showed ~10 times less raw bioluminescence radiance compared to free luciferin with SC/IP administration but with IV administration raw bioluminescence radiance was ~3–4 times higher than that of free luciferin.

Using Nano-lucDiR, both bioluminescence and fluorescence could be seen together. The application of this approach can be varied with different parameters. This strategy provides an alternative method to evaluate targeted therapeutic efficacy while monitoring tumor regression during treatment *in vivo*. Also, it enables screening of drug/nanoparticle localization in tumors *in-vivo* with high resolution, quantitatively and specifically. The characterization of nanotherapeutic particles *in-vivo* for the visualization of localization of particles *in-vivo* involves the attachment of fluorophores and the molecules of interest are inherently fluorescent (Xenolight DiR) or labeled with a fluorophore. The multimodality

imaging technique used here can effectively be used for characterizing nanoparticle activities *in-vivo* in preclinical studies.

CONCLUSION

The present study deals with the development and evaluation of nanoparticles of a well studied *in-vivo* imaging agent luciferin. The prepared Nano-Luc was optimized for its formulation and *in-vitro* parameters. The stability studies of prepared Nano-Luc determined that the shelf life of Nano-Luc was found to be more than 10 months at 25°C. Nano-Luc delivered luciferin and could express sufficient bioluminescence radiance for more than 24 h when administered by IP/SC/IV to mice (tumors) expressing luciferase. Nano-Luc Kinetic studies revealed a steady and longer release of luciferin when encapsulated as compared to free luciferin. Furthermore, Nanoluc-DiR showed possibility of tumor multimodality imaging as well as its use for characterizing nanoparticle activities *in-vivo* in preclinical studies.

ACKNOWLEDGMENTS AND DISCLOSURES

This work was financially supported by National Institute of Health - MBRS-SC1 Program (Grant # SC1 GM092779-01). The authors report no financial interest that might pose a potential, perceived, or real conflict of interest. U.S. Patent filed "Modified Nanodelivery System and Method for Enhanced *In vivo* Medical and Preclinical Imaging." (U.S. 13/851610).

REFERENCES

1. Di Carli MF, Dorbala S, Meserve J, El Fakhri G, Sitek A, Moore SC. Clinical myocardial perfusion PET/CT. J Nucl Med. 2007;48(5):783–93.
2. Mosconi L, Tsui WH, Herholz K, Pupi A, Drzezga A, Lucignani G, *et al.* Multicenter standardized 18F-FDG PET diagnosis of mild cognitive impairment, Alzheimer's disease, and other dementias. J Nucl Med. 2008;49(3):390–8.
3. Zhao B, Schwartz LH, Larson SM. Imaging surrogates of tumor response to therapy: anatomic and functional biomarkers. J Nucl Med. 2009;50(2):239–49.
4. Hillner BE, Liu D, Coleman RE, Shields AF, Gareen IF, Hanna L, *et al.* The National Oncologic PET Registry (NOPR): design and analysis plan. J Nucl Med. 2007;48(11):1901–8.
5. Hargreaves RJ. The role of molecular imaging in drug discovery and development. Clin Pharmacol Ther. 2008;83(2):349–53.
6. Niu G, Chen X. Has molecular and cellular imaging enhanced drug discovery and drug development? Drugs R D. 2008;9(6):351–68.
7. Cho H, Ackerstaff E, Carlin S, Lupu ME, Wang Y, Rizwan A, *et al.* Noninvasive multimodality imaging of the tumor microenvironment: registered dynamic magnetic resonance imaging and positron emission tomography studies of a preclinical tumor model of tumor hypoxia. Neoplasia. 2009;11(3):247–59. 2p following 59.
8. Contag CH, Ross BD. It's not just about anatomy: in vivo bioluminescence imaging as an eyepiece into biology. J Magn Reson Imaging. 2002;16(4):378–87.
9. Cai W, Chen X. Multimodality molecular imaging of tumor angiogenesis. J Nucl Med. 2008;49 Suppl 2:113S–28.
10. Lim E, Modi K, Christensen A, Meganck J, Oldfield S, Zhang N. Monitoring tumor metastases and osteolytic lesions with bioluminescence and micro CT imaging. J Vis Exp. 2011(50):2775.
11. Gross S, Piwnica-Worms D. Spying on cancer: molecular imaging in vivo with genetically encoded reporters. Cancer Cell. 2005;7(1):5–15.
12. Corn DJ, Kim Y, Krebs MD, Mounts T, Molter J, Gerson S, *et al.* Imaging Early Stage Osteogenic Differentiation of Mesenchymal Stem Cells. J Orthop Res. 2013;31(6):871–9.
13. Chan CT, Paulmurugan R, Reeves RE, Solow-Cordero D, Gambhir SS. Molecular imaging of phosphorylation events for drug development. Mol Imaging Biol. 2009;11(3):144–58.
14. Willmann JK, van Bruggen N, Dinkelborg LM, Gambhir SS. Molecular imaging in drug development. Nat Rev Drug Discov. 2008;7(7):591–607.
15. Hayashi D, Tkacz JN, Hammond S, Devenney-Cakir BC, Zaim S, Bouzegaou N, *et al.* Gastroenteropancreatic neuroendocrine tumors: multimodality imaging features with pathological correlation. Jpn J Radiol. 2011;29(2):85–91.
16. Zinn KR, Chaudhuri TR, Szafran AA, O'Quinn D, Weaver C, Dugger K, *et al.* Noninvasive bioluminescence imaging in small animals. ILAR J. 2008;49(1):103–15.
17. Sadikot RT, Blackwell TS. Bioluminescence imaging. Proc Am Thorac Soc. 2005;2(6):537–40. 11–2.
18. Badr CE, Tannous BA. Bioluminescence imaging: progress and applications. Trends Biotechnol. 2011;29(12):624–33.
19. Zhang N, Lyons S, Lim E, Lassota P. A spontaneous acinar cell carcinoma model for monitoring progression of pancreatic lesions and response to treatment through noninvasive bioluminescence imaging. Clin Cancer Res. 2009;15(15):4915–24.
20. Zhang W, Feng JQ, Harris SE, Contag PR, Stevenson DK, Contag CH. Rapid in vivo functional analysis of transgenes in mice using whole body imaging of luciferase expression. Transgenic Res. 2001;10(5):423–34.
21. Lim E, Modi KD, Kim J. In vivo bioluminescent imaging of mammary tumors using IVIS spectrum. J Vis Exp. 2009(26):1210.
22. Bhaumik S, Gambhir SS. Optical imaging of Renilla luciferase reporter gene expression in living mice. Proc Natl Acad Sci U S A. 2002;99(1):377–82.
23. Frackman S, Anhalt M, Nealson KH. Cloning, organization, and expression of the bioluminescence genes of Xenorhabdus luminescens. J Bacteriol. 1990;172(10):5767–73.
24. Siragusa GR, Nawotka K, Spilman SD, Contag PR, Contag CH. Real-time monitoring of Escherichia coli O157:H7 adherence to beef carcass surface tissues with a bioluminescent reporter. Appl Environ Microbiol. 1999;65(4):1738–45.
25. Zhao H, Doyle TC, Coquoz O, Kalish F, Rice BW, Contag CH. Emission spectra of bioluminescent reporters and interaction with mammalian tissue determine the sensitivity of detection in vivo. J Biomed Opt. 2005;10(4):41210.
26. Gross S, Abraham U, Prior JL, Herzog ED, Piwnica-Worms D. Continuous delivery of D-luciferin by implanted micro-osmotic pumps enables true real-time bioluminescence imaging of luciferase activity in vivo. Mol Imaging. 2007;6(2):121–30.
27. Hiler DJ, Greenwald ML, Geusz ME. Imaging gene expression in live transgenic mice after providing luciferin in drinking water. Photochem Photobiol Sci. 2006;5(11):1082–5.
28. Berger F, Paulmurugan R, Bhaumik S, Gambhir SS. Uptake kinetics and biodistribution of 14C-D-luciferin–a radiolabeled substrate for the firefly luciferase catalyzed bioluminescence reaction: impact on

bioluminescence based reporter gene imaging. Eur J Nucl Med Mol Imaging. 2008;35(12):2275–85.
29. Gross S, Piwnica-Worms D. Real-time imaging of ligand-induced IKK activation in intact cells and in living mice. Nat Methods. 2005;2(8):607–14.
30. Kheirolomoom A, Kruse DE, Qin S, Watson KE, Lai CY, Young LJ, *et al.* Enhanced in vivo bioluminescence imaging using liposomal luciferin delivery system. J Control Release. 2010;141(2):128–36.
31. Souto EB, Wissing SA, Barbosa CM, Muller RH. Development of a controlled release formulation based on SLN and NLC for topical clotrimazole delivery. Int J Pharm. 2004;278(1):71–7.
32. Kakkar V, Muppu SK, Chopra K, Kaur IP. Curcumin loaded solid lipid nanoparticles: an efficient formulation approach for cerebral ischemic reperfusion injury in rats. Eur J Pharm Biopharm. 2013;85(3 Pt A):339–45.
33. Muller RH, Radtke M, Wissing SA. Nanostructured lipid matrices for improved microencapsulation of drugs. Int J Pharm. 2002;242(1–2):121–8.
34. Zhang GJ, Chen TB, Davide J, Tao W, Vanko A, Connolly B, et al. Visualization of Mitotic Arrest of Cell Cycle with Bioluminescence Imaging in Living Animals. Mol Imaging Biol. 2013 Feb 26.
35. Pardeike J, Hommoss A, Muller RH. Lipid nanoparticles (SLN, NLC) in cosmetic and pharmaceutical dermal products. Int J Pharm. 2009;366(1–2):170–84.
36. Singh B, Bhatowa R, Tripathi CB, Kapil R. Developing micro-/nanoparticulate drug delivery systems using "design of experiments". Int J Pharm Investig. 2011;1(2):75–87.
37. Xiang QY, Wang MT, Chen F, Gong T, Jian YL, Zhang ZR, *et al.* Lung-targeting delivery of dexamethasone acetate loaded solid lipid nanoparticles. Arch Pharm Res. 2007;30(4):519–25.
38. Singh A, Ahmad I, Akhter S, Jain GK, Iqbal Z, Talegaonkar S, *et al.* Nanocarrier based formulation of Thymoquinone improves oral delivery: Stability assessment, in vitro and in vivo studies. Colloids Surf B: Biointerfaces. 2013;102:822–32.
39. Hao J, Wang F, Wang X, Zhang D, Bi Y, Gao Y, *et al.* Development and optimization of baicalin-loaded solid lipid nanoparticles prepared by coacervation method using central composite design. Eur J Pharm Sci. 2012;47(2):497–505.
40. Patlolla RR, Chougule M, Patel AR, Jackson T, Tata PN, Singh M. Formulation, characterization and pulmonary deposition of nebulized celecoxib encapsulated nanostructured lipid carriers. J Control Release. 2010;144(2):233–41.
41. Schwarz C, Mehnert W. Freeze-drying of drug-free and drug-loaded solid lipid nanoparticles (SLN). Int J Pharm. 1997;157(2):171–9.
42. Venkateswarlu V, Manjunath K. Preparation, characterization and in vitro release kinetics of clozapine solid lipid nanoparticles. J Control Release. 2004;95(3):627–38.
43. Puglia C, Blasi P, Rizza L, Schoubben A, Bonina F, Rossi C, *et al.* Lipid nanoparticles for prolonged topical delivery: an in vitro and in vivo investigation. Int J Pharm. 2008;357(1–2):295–304.